Complex Permittivity Model for Time Domain Reflectometry Soil Water Content Sensing: II. Calibration

R.C. Schwartz*
S.R. Evett
J.M. Bell
USDA-ARS
Conservation and Production Research Lab.
Bushland, TX 79012

Despite numerous applications of time domain reflectometry (TDR), serious difficulties in estimating accurate soil water contents under field conditions remain, especially in fine-textured soils. A complex dielectric mixing model was calibrated for fine-textured soils (24–45% clay) and its accuracy was evaluated and compared with empirical calibrations. The Ap and Bt horizons of two soils were packed into columns and adjusted to volumetric water contents (θ) ranging from air dry to near saturation. Travel time and bulk electrical conductivity (σ_0) were measured using TDR at temperatures (T) of 8, 22, and 40°C and using three coaxial cables to obtain a range of input spectrum bandwidths (ω_S). Apparent permittivities (K_a) were predicted using the complex permittivity model with measured θ, T, σ_0, ω_S, and soil bulk density, and fitted to measured K_a by optimizing specific surface area (A_s), the power-law exponent (a), and an empirical polarization loss factor. Measured K_a was best approximated using the power-law dielectric mixing model with a semiempirical effective frequency estimate and $a = 0.68$. Predicted A_s increased with increasing clay content, cation exchange capacity, and measured specific surface areas. The two-parameter power-law calibration removed temperature bias in θ estimates and reduced the RMSE in θ estimates by an average of 0.006 $m^3\ m^{-3}$ compared with an empirical calibration. Empirical models predicted field θ with oscillations of up to 0.022 $m^3\ m^{-3}$ in phase with soil temperatures resulting from permittivity temperature dependencies. In contrast, the calibrated dielectric mixing model removed or dampened in-phase θ fluctuations to <0.004 $m^3\ m^{-3}$, which permitted the detection of more subtle changes (<0.02 $m^3\ m^{-3}$) in θ.

Abbreviations: BET, Brunauer, Emmett, and Teller; RSD, residual standard deviation; TDR, time domain reflectometry.

During the past 30 yr, the development and continuing improvement of the TDR method for in situ measurement of soil water content has led to significant advances in the study of hydrologic processes within the soil profile. Much of the fundamental success of this technique was due to a broadly applicable calibration equation (Topp et al., 1980) for mineral soils that reflected the near-univariate response of measured permittivity to soil water content. Later experimental work (Ledieu et al., 1986; Herkelrath et al., 1991; Heimovaara, 1993; Topp and Reynolds, 1998) demonstrated that the square root of permittivity, or equivalently travel time, varied linearly with volumetric water content, θ. This approximation resulted in a calibration equation with a slope and intercept that were influenced in a nontrivial way by soil properties (Ferré and Topp, 2002; Robinson et al., 2003).

Although empirical approaches can provide acceptable estimates of soil water contents, the use of electromagnetic mixing models can improve the understanding of the dielectric behavior of soils and lead to more physically based calibration equations. Dobson et al. (1985) demonstrated that both a dielectric mixing formula based on a dispersion model (de Loor, 1968) and a power-law approximation (Birchak et al., 1974) were able to describe the high-frequency (>1 GHz) complex dielectric permittivity of soil. In addition to the air, mineral, and water components, Dobson et al. (1985) incorporated a bound water component into their mixing models to account for reduced polarizability of water near clay surfaces. In a later study, Heimovaara et al. (1994) used a four-component power-law mixing model to describe the complex dielectric permittivity of soils with low organic C content (≤37 g kg^{-1}). Most significantly, Heimovaara et al. (1994) demonstrated that imaginary parts of the dielectric permittivities need to be accounted for in the mixing model to correctly describe the measured apparent permittivities. In practice, most of the mixing models developed for soils have omitted the imaginary contributions of some or all of the dielectric damping mechanisms associated with bound and bulk water (Dobson et al., 1985; Roth et al., 1990; Dirksen and Dasberg, 1993; Heimovaara et al., 1994; Or and Wraith, 1999). More recently, Boyarskii et al. (2002)

The mention of trade names of commercial products is solely for the purpose of providing specific information and does not imply recommendation or endorsement by the USDA.

Soil Sci. Soc. Am. J. 73:898-909
doi:10.2136/sssaj2008-0195
Received 3 June 2008.
*Corresponding author (robert.schwartz@ars.usda.gov).
© Soil Science Society of America
677 S. Segoe Rd. Madison WI 53711 USA
All rights reserved. No part of this periodical may be reproduced or transmitted in any form or by any means, electronic or mechanical, including photocopying, recording, or any information storage and retrieval system, without permission in writing from the publisher. Permission for printing and for reprinting the material contained herein has been obtained by the publisher.

and Mironov et al. (2004) described dielectric models of soils for remote microwave applications that include both the real and imaginary components of bound and bulk water. These models were developed to provide single-frequency approximations for the high (1–18 GHz) frequency range, however, and do not consider temperature effects on the dielectric response. This limits the models for use in broadband TDR applications, especially under field conditions where temperature fluctuations are significant.

Estimation of soil water contents with TDR under field conditions introduces new sources of uncertainty that are not easily addressed using conventional calibration equations. Long cables and other hardware such as multiplexers can significantly reduce the measurement bandwidth of the signal (Logsdon, 2000, 2006), thereby changing the calibration. Measured apparent permittivities (K_a) are influenced by soil bulk densities (ρ_b), bulk electrical conductivities (σ_0), and clay contents (Jacobsen and Schjønning, 1993; Malicki et al., 1996; Persson and Berndtsson, 1998; Hook et al., 2004; Evett et al., 2005) that may differ in the field from the calibrated soils. Lastly, K_a measurements using TDR can exhibit temperature sensitivities inconsistent with those expected for bulk water (Persson and Berndtsson, 1998; Or and Wraith, 1999; Evett et al., 2005). We emphasize that all of the above difficulties with field measurements are exacerbated for high-surface-area soils (Logsdon, 2005, 2006).

Most, if not all, of the documented efforts at temperature corrections for TDR water content calibrations have been empirical (e.g., Ledieu et al., 1986; Pepin et al., 1995; Gong et al., 2003; Benson and Wang, 2006; Kahimba and Ranjan, 2007) with the notable exception of Or and Wraith (1999). Or and Wraith (1999) demonstrated that the temperature response of dielectric permittivity in soils represented the interplay among the temperature dependencies of the static permittivity of bulk water and the volumetric fraction of bound water. Evett et al. (2005) hypothesized that temperature sensitivity in soil resulted from the dependence of σ_0 on temperature and accordingly developed a calibration equation using TDR-measured σ_0.

Dielectric mixing models, when properly specified, are practical alternatives to the empirical calibrations conventionally used in field applications because soil ρ_b, σ_0, and temperature measurements can be incorporated into the calibration. Moreover, the use of specific surface area as a parameter in the mixing model (Or and Wraith, 1999) is desirable because of its physical significance and its relationship to temperature effects on apparent permittivity and to soil clay contents. Although dielectric mixing models that include imaginary components have been used under isothermal, laboratory conditions (Dobson et al., 1985; Heimovaara et al., 1994), we are unaware of documented attempts to extend these calibrations to field-measured K_a using TDR. In practice, K_a is measured and subsequently θ must be estimated based on its specification within the complex dielectric mixing model. Consequently, this transforms the straightforward calculation of K_a as a function of θ into a one-dimensional root-finding problem. A similar situation arises out of the calibration of capacitance sensors using circuit theory (Kelleners et al., 2004).

The overall goal of this study was to develop a practical model and framework to allow temperature- and frequency-dependent water content calibrations in fine-textured soils for the interpretation of routine TDR measurements in the field. The specific objectives of this study were to calibrate the complex dielectric mixing models presented by Schwartz et al. (2009) for the Ap and Bt horizons of two fine-textured soils, compare water content estimation errors of this physically based model with conventional calibration equations, and evaluate the complex dielectric mixing models' performance under field conditions.

MATERIALS AND METHODS

Soils were collected from the Ap (0–0.15 m) and Bt (0.15–0.30) horizons of a Pullman silty clay loam (a fine, mixed, superactive, thermic Torrertic Paleustoll) in Bushland, TX, and a Richfield silt loam (a fine, smectitic, mesic Aridic Argiustoll) in Tribune, KS. Smectite and mica (illite) dominate the clay fractions of these soil horizons (Soil Survey Staff, 2008). Clay contents of the sampled soils (Table 1) determined using the hydrometer method (Gee and Or, 2002) ranged from 24 to 45%. The specific surface area of oven-dry (105°C), 2-mm sieved soil was estimated using an automated analyzer (Quantachrome Nova, Boynton Beach, FL) with N_2 adsorbate in conjunction with the Brunauer, Emmett, and Teller (BET) equation. A multipoint surface area estimation was calculated based on the gas volume measurements across a range of six relative vapor pressures (Pennell, 2002). The specific surface area was also determined by bringing 5 g of 2-mm sieved soil into equilibrium with deionized water in a humidity chamber. Subsequently, the samples were placed in a closed chamber containing saturated $MgNO_3$ at 20°C corresponding to a relative humidity of 54.4% (Greenspan, 1977) and permitted to equilibrate for a period of approximately 2 wk. Specific surface area was calculated based on the gravimetric water content of the equilibrated samples assuming a monolayer of water molecules with 0.3-nm thickness (Logsdon, 2005).

Soils were sieved through a 12.7- by 12.7-mm mesh screen and packed in 0.2-m-diam. by 0.21-m-long Schedule 40 polyvinyl chloride

Table 1. Physical soil properties and fitted parameters describing electrical conductivity with respect to saturation and temperature.†

Soil	Texture	Clay	Sand	CEC‡	A_s§ (N_2)	A_s§ (H_2O)	ρ_b	σ_{25}	n	Δ
		—— % ——		cmol kg^{-1}	—— m^2 g^{-1} ——		kg m^{-3}	S m^{-1}		K^{-1}
Pullman Ap	silty clay	39.4	16.5	24.0	48.2	249	1370	0.114	1.180	0.0224
Pullman Bt	silty clay	45.0	13.2	28.5	61.0	293	1350	0.148	1.613	0.0246
Richfield Ap	silt loam	24.3	15.7	18.9	35.0	182	1330	0.106	0.985	0.0247
Richfield Bt	silty clay loam	34.3	14.2	24.0	47.3	240	1250	0.118	1.196	0.0234

† Particle-size distributions, cation exchange capacities (CEC), and specific surface areas (A_s) represent the average of two samples; bulk density (ρ_b) reflects the average bulk density of packed columns; σ_{25} is the bulk direct-current conductivity at saturation and 25°C, n is a fitted empirical exponent, and Δ is a multiplier to account for the response of electrical conductivity to temperature.

‡ Determined using pH 7 buffered NH_4OAc displacement solution.

§ Determined using N_2 gas adsorbate with the BET (Brunauer, Emmett, and Teller) equation (Pennell, 2002) and by using deionized water (H_2O) with soils equilibrated at 54.4% relative humidity (Logsdon, 2005).

Table 2. Physical and electrical properties of coaxial cables, cabling system, and time domain reflectometry probe. All measurements are averages of at least five acquired waveforms.

Coaxial cable between reflectometer and multiplexer		Cabling system response†		Probe characteristics associated with cabling system‡					
Cable make (all 50 Ω)	Length	τ_c	ω_S	$t_1 - t_{bis}$	ρ_{air}	ρ_{sc}	K_p§	Z_g	L_e¶
	m	ns	rad GHz	ns			m^{-1}	Ω	m
RG 8/U (Belden 9913)	1.5	0.350	4.04	0.493	1.0086	−0.9573	3.117	234.9	0.1983
RG 8/U (Belden 9913)	12.0	0.495	2.85	0.541	1.0056	−0.9807	3.208	241.7	0.1986
RG 58A/U (Alpha 9058AC)	12.0	1.758	0.80	0.693	0.9963	−0.9635	3.213	242.1	0.1976

† τ_c, fitted time constant obtained from the open-ended reflection at the termination of the cable; wS, corresponding input spectrum bandwidth (see Schwartz et al., 2009).

‡ t_1, time when the pulse exits the probe handle; t_{bis}, time corresponding to the intersection of the tangent of the first rising limb and the preceding base-line tangent; ρ_{air}, reflection coefficient of the probe in air; ρ_{sc}, reflection coefficient of the short-circuited probe; K_p, probe constant; Zg, probe characteristic impedance; L_e, electrical probe length.

§ Theoretical probe constant is 3.2324 m^{-1} based on a derivation by Paolo Castiglione (personal communication. 2008).

¶ Electrical length of the probe is based on measured travel time in water assuming a static dielectric constant of 79.49 at 22°C (Stogryn, 1995). The physical length of the probe used in these measurements was 0.199 ± 0.001 m.

columns. After soils were packed, trifilar probes (0.2-m length) were installed vertically into the prepared soil columns. The trifilar probes had rod diameters of 3.2 mm and an outer rod separation distance of 60 mm. Three replicate columns were prepared for each water content level. A range of volumetric water contents were obtained using two methods. Volumetric water contents $\lesssim$0.20 m^3 m^{-3} were achieved by combining air-dry soil with different ratios of deionized water, thoroughly mixing to achieve uniformity, and packing the mixture into the columns in 20-mm increments. For water contents $\gtrsim$0.25 m^3 m^{-3}, air-dry soil was packed into the columns in 20-mm increments, after which the soil was saturated from the bottom with 0.001 mol L^{-1} $CaSO_4$. In this case, water contents were adjusted through a combination of drainage (at water contents near saturation) and short, 4-h periods of evaporation, after which the columns were sealed and permitted to equilibrate. Evaporative drying of the entire length of the column was accommodated during these periods by drawing a small vacuum through the bottom of the column to establish air flow. Equilibrium was assumed to be attained when a negligible change in permittivity with time was recorded after a minimum of 1 wk. This process was repeated until the desired water contents were achieved, which, at the lower water contents, took in excess of a month for the Bt horizons.

Waveforms were acquired using a Tektronix 1502C cable tester (Tektronix, Beaverton, OR). For every cabling setup, the lead 3-m RG 58 coaxial cable attached to the TDR probe was connected to a 16-port coaxial multiplexer (Model TR-200, Dynamax, Houston, TX; Evett, 1998). A range of bandwidths was achieved by using three coaxial cables (Table 2) that connected the multiplexer to the cable tester. Four replicate travel time and apparent bulk electrical conductivity measurements were taken at room temperature (22–23°C), in a refrigerator (6–8°C), and in a water-jacketed incubator (40–42°C). Except for the first 0.5 m of the coaxial cable connected to the probe, all cables and connections were maintained at room temperature. Time domain reflectometry measurements were completed after 2 d of equilibration under each temperature regime. Travel time measurements were recorded for each cable and each of the three replicate columns at every water content and temperature combination. After each set of measurements at a given temperature regime, the columns were weighed on a 30-kg (±1 g) balance. Upon completion of TDR measurements for a given column, the soil was removed, weighed, air dried in a 40°C oven for 3 d, and weighed again. Subsamples of the air-dried soils were oven dried (105°C) to determine the bulk density and the final gravimetric and volumetric water contents of the soil in the column. Based on the maximum calculated 95% confidence interval of 0.007 kg kg^{-1} for the gravimetric water content of soils packed into columns, errors in measured water contents were <0.01 m^3 m^{-3}.

Waveforms were interpreted to estimate travel times using the TACQ software (Evett, 2000a,b). Because of the difficulty in identifying the time, t_1, when the step pulse exited the probe handle at low soil water contents, t_1 was estimated by adding a fixed offset to t_{bis}, the time defined by the intersection of the tangent to the rising limb and the preceding baseline tangent. Fixed offsets ($t_1 - t_{bis}$) were estimated at large soil water contents (~0.40 m^3 m^{-3}) and were influenced by coaxial cables (Table 2), probably because low pass filtering by lossy cables increased the travel time through the epoxy probe handle. The time associated with the second reflection was estimated by the intersection of the baseline tangent (20 points) with the rising limb tangent (11 points). The stop point of the baseline tangent was set to 65% at low soil water contents (<0.25 m^3 m^{-3}) and the default of 75% at greater soil water contents. All other parameters used to estimate travel time were set to the default values used by the TACQ software (Evett, 2000a,b). The use of these waveform interpretation methods for the three coaxial cables yielded an average electrical length L_e of 0.1982 m (±0.0005 SD) for a single probe in deionized water that did not vary significantly from its measured physical length of 0.199 ± 0.001 m (Table 2). Therefore, we used L_e = 0.20 m for all calculations to represent the probe length, which varied from 0.199 to 0.201 m in this study.

The bandwidth associated with each cable setup was determined from the signal rise time at the termination of the 3-m lead RG 58 cable with the TDR probe removed. The same multiplexer, interconnects, and cables used to measure the travel time were also included in the circuit. Using the unit step response function (Kaiser, 2005) with time, t_0 (ns), and amplitude, V_0, offsets,

$$\frac{V-V_0}{V_{100}-V_0}=1-\exp\left(-\frac{t-t_0}{\tau_c}\right) \qquad [1]$$

the mean transition duration of the pulse τ_c (ns) and the 100% amplitude level V_{100} were fitted to the measured open-ended reflection (Fig. 1). The effective bandwidth of the pulse at the termination of the coaxial cable, ω_S (rad s^{-1}), was calculated as per Schwartz et al. (2009) and decreased with increasing cable length (Table 2) and increasing cable manufacturer attenuation rating (98 and 360 dB km^{-1} at 400 MHz for the RG 8/U and RG 58A/U cables, respectively).

Bulk electrical conductivity measurements were completed using the procedure of Castiglione and Shouse (2003) with cable-specific air

and short-circuit reflection coefficients. Short-circuit measurements were completed by clamping two Al plates together with the probe rods sandwiched between at the midpoint of the rod length. Probes were calibrated at a temperature of 22°C in deionized water and four reference KCl solutions (2.5, 5.0, 7.5, and 10.0 mmol L^{-1}, equivalent to 0.035, 0.070, 0.106, and 0.141 S m^{-1}, respectively, at 25°C). Electrical conductivity of the solutions was measured independently with a standard electrical conductivity meter calibrated using the same KCl solutions. The probe constant K_p was estimated by finding the slope of the scaled reflection coefficient (Castiglione and Shouse, 2003) vs. the measured conductivity and multiplying by the cable characteristic impedance (50 Ω). Calculated probe constants were within 4% of the theoretical constant for these probes (Table 2). The predicted σ_0 in response to the saturation ratio and temperature was evaluated by fitting an empirical equation to the measured electrical conductivity data (Fig. 2). Estimated parameters describing the σ_0 response (Table 1) were used to plot trend lines of K_a as a function of θ, which would otherwise be discontinuous if the actual σ_0 measurements were used.

The frequency- and temperature-dependent complex dielectric permittivity of the soil, $\varepsilon^*(\omega,T)$, was described using a power-law mixing model (Birchak et al., 1974; Dobson et al., 1985; Dirksen and Dasberg, 1993) in combination with the imaginary conductive loss component to yield

$$\varepsilon^*(\omega,T)=\left[\begin{array}{l}\left(1-\frac{\rho_b}{\rho_s}-\theta\right)(\varepsilon_a)^a+\frac{\rho_b}{\rho_s}(\varepsilon_s)^a+\\(\theta-\theta_{bw})\left[\varepsilon_{fw}^*(\omega,T)\right]^a+\\\theta_{bw}\left[\varepsilon_{bw}^*(\omega,T)\right]^a\end{array}\right]^{1/a}-j\frac{\sigma_0}{\omega\varepsilon_0} \qquad [2]$$

where ω is angular frequency (rad s^{-1}), T is soil temperature, σ_0 is direct-current bulk electrical conductivity (S m^{-1}), ε_a is gas-phase permittivity, ε_s is solid-phase permittivity, $\varepsilon_{fw}^*(\omega,T)$ is bulk (free) water complex permittivity, $\varepsilon_{bw}^*(\omega,T)$ is bound water complex permittivity, ρ_b is soil bulk density (kg m^{-3}), ρ_s is particle density (kg m^{-3}), θ is volumetric soil water content (m^3 m^{-3}), θ_{bw} is volume fraction of bound soil water (m^3 m^{-3}), which is a function of the specific surface area A_s (m^2 kg^{-1}), a is a fitted empirical exponent, ε_0 is vacuum electric permittivity (8.854×10^{-12} F m^{-1}), and $j = \sqrt{-1}$. The complex permittivities of free and bound water are calculated based on the equations given by Schwartz et al. (2009, Eq. [6] and [11]). In addition, the volumetric fraction of bound soil water is calculated as a function of ρ_b and A_s (Schwartz et al., 2009, Eq. [12] and [13]). We also considered the four-component dielectric mixing model of de Loor (1968), which assumes soil to be represented by an isotropic mixture of platelike particles, expressed as (Dobson et al., 1985)

$$\varepsilon^*(\omega,T)=\frac{\begin{array}{l}3\varepsilon_s+2(\theta-\theta_{bw})\left[\varepsilon_{fw}^*(\omega,T)-\varepsilon_s\right]+\\2\theta_{bw}\left[\varepsilon_{bw}^*(\omega,T)-\varepsilon_s\right]+\\2\left(1-\frac{\rho_b}{\rho_s}-\theta\right)(\varepsilon_a-\varepsilon_s)\end{array}}{\begin{array}{l}3+(\theta-\theta_{bw})\left[\frac{\varepsilon_s}{\varepsilon_{fw}^*(\omega,T)}-1\right]+\\\theta_{bw}\left[\frac{\varepsilon_s}{\varepsilon_{bw}^*(\omega,T)}-1\right]+\\\left(1-\frac{\rho_b}{\rho_s}-\theta\right)\left(\frac{\varepsilon_s}{\varepsilon_a}-1\right)\end{array}}-j\frac{\sigma_0}{\omega\varepsilon_0} \qquad [3]$$

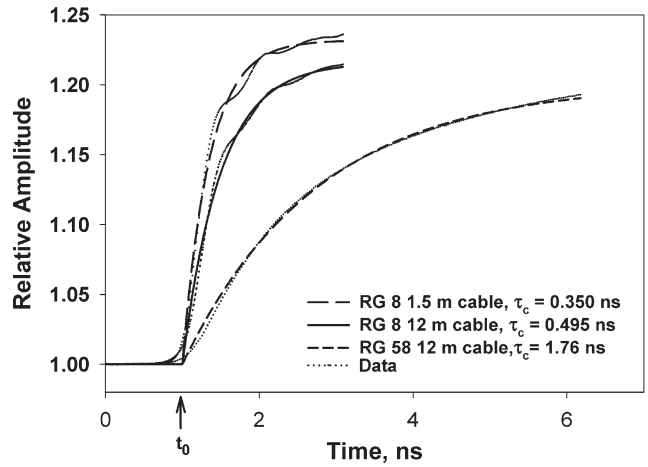

Fig. 1. Open-ended coaxial cable reflections with three cables interposed between the cable tester and multiplexer; τ_c is the fitted mean transition duration of the pulse and t_0 is the time offset from zero.

and hereafter referred to as the de Loor–Dobson dielectric mixing model. In both mixing models, bulk and bound water complex permittivity can be described using the Debye or Cole–Davidson relaxation equations, respectively (Schwartz et al., 2009). Calculation of the volume fraction and permittivity of bound water requires an estimate of the specific surface area A_s (m^2 kg^{-1}) and the Cole–Davidson distribution coefficient (β_{CD}), which are fitted parameters. In addition, we used a single-frequency approximation to estimate permittivity, which requires the substitution of an effective frequency for ω in Eq. [2] and [3].

We considered two approaches to estimate the center or effective frequency of the attenuated pulse, ω_R. A direct calculation of effective frequency was based on the integral formula for the centroid of the amplitude spectrum (Schwartz et al., 2009):

$$\omega_R=\frac{\int_0^\infty S(\omega,\omega_S)\exp[-\alpha(\omega)2L]\omega d\omega}{\int_0^\infty S(\omega,\omega_S)\exp[-\alpha(\omega)2L]d\omega} \qquad [4]$$

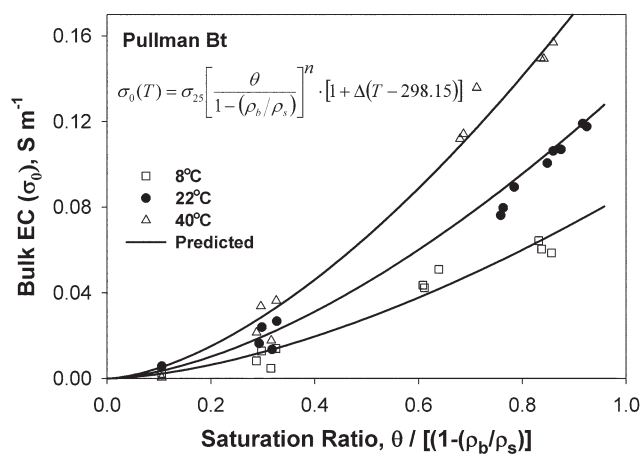

Fig. 2. Predicted and measured bulk electrical conductivity σ_0 response to soil water saturation and temperature (T) for the Pullman Bt horizon. Predicted response was calculated using the fitted coefficients in Table 1; σ_{25} is the bulk direct-current conductivity at saturation and 25°C, n is a fitted empirical exponent, △ is a multiplier to account for the response of electrical conductivity to temperature, θ is volumetric soil water content, ρ_b is soil bulk density, and ρ_s is soil particle density.

Table 3. Vector of optimized parameters† β for combinations of mixing model and effective frequency calculations.

Effective frequency calculation	Dielectric mixing model	
	Power-law Eq. [2]	de Loor–Dobson Eq. [3]
Eq. [4]	A_s, a, β_{CD}	A_s, β_{CD}
Eq. [5]	A_s, a, p, m	A_s, p, m

† Specific surface area (A_s), power-law mixing exponent (a), Cole–Davidson distribution coefficient (β_{CD}), polarization loss factor (p), and an exponent to describe the increase in polarization losses with volumetric water content (m).

where $S(\omega,\omega_S)$ is the input amplitude spectrum described by a third-order Butterworth filter with bandwidth ω_S, L is the length of the TDR probe (m), and $\alpha(\omega)$ is the attenuation factor, which can be evaluated using one of the mixing models across a range of frequencies (Schwartz et al., 2009). Alternatively, with the assumption that attenuation increases linearly with frequency, we derived an approximate effective frequency (Schwartz et al., 2009) as

$$\omega_R = \frac{\omega_{R1}(\omega_S)}{1+2L7.442\times10^5\left\{\alpha_2\left[\omega_{R1}(\omega_S)\right]\right\}\times\left[\omega_{R1}(\omega_S)\right]^{-0.5904}} \quad [5]$$

where $\alpha_2(\omega)$ is the attenuation function associated with the polarization of bulk water evaluated at the angular frequency of $\omega = \omega_{R1}(\omega_S)$ resulting from losses associated with bound water:

$$\omega_{R1}(\omega_S) = \frac{\omega_S}{1+\omega_S L p \theta^m \sqrt{\mu_0\varepsilon_0 / \mathrm{Re}\left[\varepsilon^*(\omega,T)\right]}} \quad [6]$$

where p is a fitted polarization loss factor ($m^3\ m^{-3}$) related to the imaginary permittivity of bound water (Schwartz et al., 2009), m is a dimensionless empirical coefficient, and μ_0 is the vacuum magnetic permittivity (1.257×10^{-6} H m^{-1}). Once the effective frequency ω_R is calculated using either of the two methods, the single-frequency approximation of apparent permittivity was calculated as

$$K_a(\omega_R,T) = \frac{\mathrm{Re}\left[\varepsilon^*(\omega_R,T)\right]}{2}\left(1+\sqrt{\left\{\frac{-\mathrm{Im}\left[\varepsilon^*(\omega_R,T)\right]}{\mathrm{Re}\left[\varepsilon^*(\omega_R,T)\right]}\right\}^2+1}\right) \quad [7]$$

It is important to recognize that the only difference between K_a calculated using the direct approach to evaluate the effective frequency (Eq. [4]) and the approximate solution (Eq. [5]) is that the effective frequency using the former approach is directly coupled to the dielectric mixing model. In contrast, the approximate solution is not coupled to the mixing models. Consequently, a change in any of the variables or parameters within the mixing model that results in a change in dielectric losses will not influence the calculated frequency decline in Eq. [5]. A detailed description of the derivations and algorithms used to calculate the apparent permittivity of the soil is given by Schwartz et al. (2009).

Given the measured values of soil water content, temperature, bulk electrical conductivity, bulk density, and the bandwidth of the input spectrum, K_a can be calculated using Eq. [7] with estimates of the vector of parameters to be optimized $\boldsymbol{\beta}$, which varies based on the selected mixing model and frequency calculation (Table 3). All other parameters in the model were held constant (Table 4). Parameters were optimized by minimization of the objective function:

$$\Phi(\beta,\chi) = \sum_{i=1}^{N}\left[\sqrt{K_a(\chi_i)} - \sqrt{\hat{K}_a(\beta,\chi_i)}\right]^2 \quad [8]$$

where K_a is the permittivity based on travel time measurements, $\hat{K}_a$ is the predicted permittivity in Eq. [7], and χ_i is the vector of independent variables (θ, T, σ_0, ρ_b, and ω_S) for i = 1 to N observations. The objective function is formulated above using the square root of permittivity because initial calculations demonstrated that this results in a lower sum of squared error in water contents. Minimization of the objective function was implemented using an adaptive, model-trust region method of nonlinear, least squares parameter optimization (Dennis et al., 1981; Dennis and Schnabel, 1983).

The calculation of apparent permittivity in Eq. [7] was based on known soil water contents; however, in practice, water contents must be estimated from the measured values of apparent permittivity. Consequently, this transforms the straightforward calculation of apparent permittivity into a one-dimensional root-finding problem for the function $f(\theta)$, defined as

$$f(\theta) = K_a - \hat{K}_a(\theta,T,\sigma_0,\rho_b,\omega_S) \quad [9]$$

where K_a is the permittivity based on travel time measurements and $\hat{K}_a$ is the predicted permittivity in Eq. [7]. We used bisection (Press et al., 1992) to solve the root problem with θ bracketed between 0 and 0.6 $m^3\ m^{-3}$. Initial evaluations of the root-finding problem revealed difficulties at very low water contents (<0.05 $m^3\ m^{-3}$) where roots converged to negative water contents and where Eq. [7] is computationally unstable and physically unrealistic. Inspection showed that the mixing models overestimated permittivities at these very low water contents. Such a result is probably due to the failure of the mixing models to correctly predict composite dielectric permittivity at low water contents (Robinson, 2004) and potentially differing dielectric response and solid interaction with interlayer water compared with water adsorbed to exterior clay surfaces. Fitting a second-order polynomial equation to the measured $K_a(\theta)$ data of both Bt horizons permitted the calculation of the intercept $K_a(0) \sim 2$, which, when substituted into the power-law mixing equation, yielded a solid-phase permittivity of 3.2 for a bulk density of 1.35 Mg m^{-3} and a power-law mixing exponent a = 0.5 to 0.65. Based on these results, we calculated an apparent solid-phase permittivity (ε_{sa}) as

$$\varepsilon_{sa} = \begin{cases} \varepsilon_s & \theta > \theta_{bw}/3 \\ 3.2 + \dfrac{3\theta}{\theta_{bw}}(\varepsilon_s - 3.2) & \theta \le \theta_{bw}/3 \end{cases} \quad [10]$$

Table 4. Constants used in model optimizations and simulations.

Parameter and value	Description
L = 0.2 m	Physical length of probe
r = 0.25 nm	Effective radius of water molecule
δ_L = 0.75 nm	Maximum thickness of the bound water region
ε_∞ = 3.2	Dielectric constant of bulk and bound water at infinite frequencies
ε_a = 1.0	Relative dielectric permittivity of air
ε_s = 5.0	Relative dielectric permittivity of the solid soil phase
ρ_s = 2650 kg m^{-3}	Particle density of soil

and substituted for ε_s into both mixing models. For all calibrations, we assumed that the solid-phase dielectric permittivity of soil, ε_s, was 5.0. This modified calculation was used for all simulations and model fits. It resulted in negligible changes in estimated permittivities and model fits but permitted the evaluation of the roots in Eq. [9] with no convergence failures.

RESULTS AND DISCUSSION

Nonlinear least squares optimizations were completed for each of the three cable setups associated with a single bandwidth (Table 2), all of the cable setups simultaneously, and only the RG 8 cables. Optimizations based on different coaxial cable data sets were examined to evaluate the influence of bandwidth on fitted parameter values and model errors. Initially, optimizations were completed for all mixing models where parameters β_{CD}, p, and m were fitted. Parameters p and m directly influence the calculation of the effective frequency (Eq. [6]), whereas β_{CD} influences the frequency response of bound water, which, in turn, affects the calculated effective frequency. The distribution coefficient β_{CD} typically converged to values greater than unity (which is physically unrealistic) and had little influence on the resulting solution. The empirical parameter m converged to values both greater and less than unity and with slightly better fits than with $m = 1$, but with greater uncertainties in the parameter estimates. Based on these initial results, we fixed both β_{CD} and m to unity to avoid overparameterization. With $\beta_{CD} = 1$, the relaxation equation describing the complex permittivity of the bound water fraction (Schwartz et al., 2009) reverts to the Debye model for a given distance from the mineral surface.

In all optimizations of the power-law mixing model, the exponent a was positively correlated with the specific surface area, A_s (Fig. 3a). Optimization of synthetic data calculated using $A_s = 200$ m^2 g^{-1} and $a = 0.68$ (Fig. 3b) demonstrated that K_a was predicted with small errors using $a = 0.80$ and a fitted A_s of 268 m^2 g^{-1}. These results suggest that, for the error levels associated with our measurements, A_s is not uniquely defined when fitted simultaneously with the power-law exponent a. To avoid this problem, we fixed $a = 0.68$, which represents the midpoint of the fitted range (Fig. 3a). This is similar to the value of $a = 0.65$ used by Dobson et al. (1985) and an average value of $a = 0.63$ obtained by Or and Wraith (1999).

For the remaining analysis and discussion, we consider the optimizations that include both RG 8 cables (1.5- and 12-m lengths, Tables 5 and 6) because they reflect the combined model performance for two input spectrum bandwidths and hence a wider range of effective frequencies. The data obtained using the 12-m RG 58 cable are not included in these optimizations because of the potential for large errors in travel time estimation as a result of significant signal attenuation. Wraith and Or (1999) discussed in detail the difficulties of travel time estimation in the presence of signal attenuation and the concomitant decrease in the slope of the second reflection. In the present study, complete attenuation of waveforms was observed for the near-saturated Pullman Bt soil at 40°C using the 12-m RG 58 cable. Although, the RG 58 data are not included in the model calibration, the dielectric response for this cable can be predicted using the mixing model, as elaborated below.

Optimizations with a fixed to a value of 0.68 resulted in both small increases (<11%) and decreases in the residual standard deviation (RSD, Table 6b) for fits in which the effective frequency was calculated using an empirical equation (Eq. [5]). When a was constrained to 0.68, however, RSD increased up to 60% for optimizations using the direct approach to evaluate the effective frequency (Eq. [4]) (Table 5b). Indeed, all optimizations using the direct approach to calculate the effective frequency (Table 5) had consistently greater RSDs than the empirical method (Table 6), independent of the number of fitting parameters or the choice of mixing model. Apparently, directly coupling the effective frequency to the mixing model reduced the flexibility of the model to simultaneously accommodate frequency-dependent attenuation and bound water effects on the apparent permittivity. This may have been a result of the simplified assumptions used in the derivation of the dielectric response of bound water across a range of frequencies and the associated dielectric damping, the principal mechanism responsible for the decline in effective frequency. Alternatively, a fitted specific surface area that is well suited for a single-frequency approximation of apparent permittivity may be poorly suited to describing attenuation across a wide range in frequencies. Despite these difficulties in using the direct calculation of effective frequency (Eq. [4]), we note that using this approach to calculate the apparent permittivity reduced the RSD by at least 15% compared with optimizations where frequency was constrained to the bandwidth of the input spectrum, ω_S (Table 2). This highlights the importance of including within the calibration equation a means to account for loss of bandwidth during pulse propagation.

Optimizations using the uncoupled, empirical frequency approximation (Eq. [5]) for both the de Loor–Dobson and

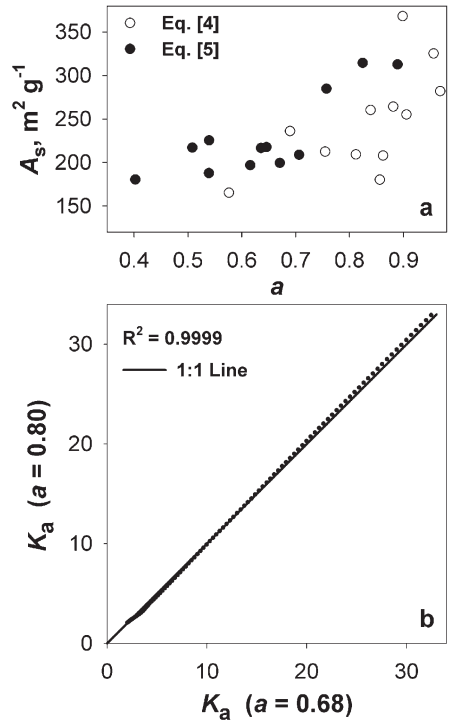

Fig. 3. Dependence of the fitted mixing-law exponent a on the fitted surface area A_s for (a) nonlinear least square results with effective frequency ω_R calculated using Eq. [4] and [5] for three cables and four soils and (b) as demonstrated by the nearly equivalent apparent permittivities K_a calculated using $A_s = 200$ m^2 g^{-1} and $a = 0.68$ (x axis), and $A_s = 268$ m^2 g^{-1} and $a = 0.80$ (y axis).

Table 5. Nonlinear least square results for the apparent permittivity fit for both RG 8 cables using the fitted specific surface area (A_s) and the power-law mixing model exponent (a). Effective frequency was calculated using Eq. [4] and a distribution coefficient of β_{CD} = 1.

Soil	RSD†	A_s	a
		$m^2\ g^{-1}$	
(a) Power-Law dielectric mixing model			
Pullman Ap	0.1300	223.5 ± 27.7‡	0.765 ± 0.042
Pullman Bt	0.2047	310.8 ± 31.1	0.981 ± 0.067
Richfield Ap	0.0867	209.8 ± 16.5	0.781 ± 0.027
Richfield Bt	0.1134	257.3 ± 17.6	0.872 ± 0.030
(b) Power-law dielectric mixing model, a = 0.68			
Pullman Ap	0.1414	172.8 ± 14.9	0.68
Pullman Bt	0.3002	159.6 ± 31.4	0.68
Richfield Ap	0.1081	153.1 ± 10.5	0.68
Richfield Bt	0.1817	152.1 ± 15.1	0.68
(c) de Loor–Dobson dielectric mixing model			
Pullman Ap	0.1831	74.3 ± 13.7	
Pullman Bt	0.3425	56.0 ± 27.6	
Richfield Ap	0.1788	43.4 ± 13.0	
Richfield Bt	0.2802	45.8 ± 17.4	

† Residual standard deviation (square root of the sum of squared errors divided by the degrees of freedom).

‡ Fitted parameters ± 95% confidence intervals.

power-law (a = 0.68) mixing models yielded fitted specific surface areas that increased with increasing measured surface areas (Tables 1, 6b, and 6c). For the power-law dielectric mixing model (Table 6b), the fitted specific surface area (n = 4) was closely correlated with clay content (r = 0.953), cation exchange capacity (r = 0.996), BET specific surface area (r = 0.998), and specific surface area determined by the mass of water retained at 54.4% relative humidity (r = 0.989). The fitted surface area of the Pullman Ap was smaller than expected based on clay content, probably because mica (illite) is the dominant clay for this horizon whereas smectite typically dominates the clay fractions of the remaining horizons (Soil Survey Staff, 2008). The polarization loss factor, p, increased with increasing clay contents and BET surface areas (Tables 1 and 6), yet again with the exception of the Pullman Ap soil. Because of the involvement of colloid surface area in the magnitude of dielectric damping, the polarization loss factor is expected to increase with increasing clay content. The close correlation of the fitted specific surface area with clay content for these soils of similar mineralogy suggests the potential of using field-measured clay contents to adjust laboratory water content calibrations completed for a representative soil horizon.

The choice of the dielectric mixing model used in the optimizations influenced the magnitude of the fitted specific surface area (Table 6). Optimizations with the power-law model yielded values of A_s that were 1.7 to 2.0 times larger than fits using the de Loor–Dobson model. Assuming specific surface areas of smectite and mica of 800 and 100 $m^2\ g^{-1}$, respectively (Fanning et al., 1989; Borchardt, 1989), and a clay fraction with no more than 70% smectite, the expected surface areas would range from 100 to 270 $m^2\ g^{-1}$ for these soils. Hence, either the de Loor–Dobson or power-law (with a = 0.68) model fits yield surface area estimates with an acceptable magnitude. The magnitude of the fitted surface area obtained using the power-law mixing model (a = 0.68; Table 6b) differed by <10% from the specific surface area determined from the mass of water retained at 54.4% relative humidity (Table 1). We note, however, that whatever means used to obtain the specific surface area, the measured or derived value is subject to some uncertainty. We have assumed that the water retained by clay at 54.4% humidity forms a monomolecular layer ~0.3 nm thick (Newman, 1983; Logsdon, 2005). Based on the work by Quirk and Murray (1999), however, water adsorbed to clay on exterior surfaces of micas and kaolinites may be two layers thick at a relative humidity of 47%. The dielectric mixing model assumes a monomolecular layer of 0.5-nm thickness and that the surface modifies the dielectric properties of water at a maximum distance of 0.75 nm (Table 4). The choice of these physical values will obviously influence the magnitude of the fitted surface area. A caveat for the interpretations of the fitted results is that the surface-induced reduction in viscosity conceptualized by Or and Wraith (1999) and applied to describe bound water effects here is only one of the mechanisms by which clays can restrict the rotational mobility of water molecules. Counterions in the diffuse double layer can also reduce static permittivity by the formation of hydrated shells of water molecules around the ions, with these molecules exhibiting restricted orientational polarizability (Sposito and Prost, 1982; Friedman et al., 2006). These cation-specific effects are not explicitly considered in the physical model and hence, given these uncertainties, the specific surface area A_s should be considered a fitted parameter that depends on the mineralogy of the soil and, to a lesser extent, the charge density and valency of the dominant saturating cations. Because of the consistently lower RSDs obtained for optimizations using the power-law mixing model with a = 0.68 (Table 6b), we subsequently examined in more

Table 6. Nonlinear least square results for the apparent permittivity fit for both RG 8 cables using the fitted specific surface area (A_s), the power-law mixing model exponent (a), and an empirical coefficient describing bound water polarization (p). Effective frequency was calculated using Eq. [5] and a bound water polarization exponent m = 1.

Soil	RSD†	A_s	a	p
		$m^2\ g^{-1}$		$m^3\ m^{-3}$
(a) Power-law dielectric mixing model				
Pullman Ap	0.1125	202.3 ± 49.7‡	0.588 ± 0.095	22.34 ± 3.87
Pullman Bt	0.1650	269.5 ± 115.2	0.645 ± 0.220	28.46 ± 4.20
Richfield Ap	0.0827	200.5 ± 30.6	0.682 ± 0.065	17.65 ± 2.93
Richfield Bt	0.0858	299.8 ± 23.3	0.823 ± 0.053	19.45 ± 2.22
(b) Power-law dielectric mixing model, a = 0.68				
Pullman Ap	0.1138	240.7 ± 26.2	0.680	19.49 ± 2.82
Pullman Bt	0.1639	286.4 ± 38.1	0.680	27.95 ± 2.54
Richfield Ap	0.0822	199.8 ± 15.7	0.680	17.70 ± 2.00
Richfield Bt	0.0954	243.2 ± 16.2	0.680	23.59 ± 1.56
(c) de Loor–Dobson dielectric mixing model				
Pullman Ap	0.1271	135.2 ± 20.5		20.55 ± 2.74
Pullman Bt	0.1650	164.2 ± 29.6		27.98 ± 2.47
Richfield Ap	0.0853	102.0 ± 11.0		22.07 ± 1.57
Richfield Bt	0.1215	126.8 ± 15.4		27.38 ± 1.63

† Residual standard deviation (square root of the sum of squared errors divided by the degrees of freedom).

‡ Fitted parameters ± 95% confidence intervals.

detail the apparent permittivity and soil water content predictions using these fitted parameters.

Solving for apparent permittivity using the fitted coefficients of the power-law mixing model (Table 6b) with σ_0 calculated using the parameters given in Table 1 with the expression given by Schwartz et al. (2009, Eq. [21]) and at soil temperatures of 8, 22, and 40°C yielded the fitted K_a–θ curves shown in Fig. 4 for the Pullman and Richfield Bt horizons. Also plotted in Fig. 4 are the measured results, which, because of errors in the σ_0 model, exhibited larger deviations from the fitted curves than optimizations with measured σ_0 would indicate. At an input spectrum bandwidth of 2.85 rad GHz (0.454 GHz), the measured results at each temperature are generally well described by the plotted trends. At a bandwidth of 0.80 rad GHz (128 MHz), where curves represent the predicted responses because these data were not included in the optimizations (Table 6b), the measured responses were more scattered about the plotted trends, especially at large water contents and 40°C. In general, the predicted permittivities agreed closely with the measured permittivities up to a maximum bulk electrical conductivity of 0.12 S m^{-1} and loss tangent of 1.7 for the Pullman Bt Horizon. These losses are associated with a predicted effective frequency of 340 rad MHz (54 MHz). At greater bulk electrical conductivities and correspondingly greater loss tangents, errors in predicted water contents increased up to 0.06 m^3 m^{-3}. Errors at high loss tangents are attributable to the difficulty in estimating the travel time in the presence of significant attenuation and the concomitant decrease in magnitude of the slope of the second reflection (Wraith and Or, 1999). At a predicted loss tangent of 2.4 (σ_0 = 0.15 S m^{-1}), the second reflection disappeared altogether for the Pullman Bt horizon at 40°C and near saturation using the 12-m RG 58 cable.

Soils were also calibrated using the empirical relationship between $\sqrt{K_a}$ and θ (Topp and Reynolds, 1998) to fit an intercept (b_0) and slope (b_1) using linear regression and the measured data from all of the cables (Table 7). Root mean square errors of the predicted water contents for these empirical calibrations were 0.003 to 0.009 m^3 m^{-3} greater than those obtained for the mixing model calibration (Table 6b). Even though the dielectric mixing model was calibrated only for the RG 8 cables, the RMSEs reported in Table 7 include data from all cables. The trends in measured and predicted soil water contents (Fig. 5) illustrate a significant temperature bias in the empirical calibration. In contrast, a temperature bias was not discerned for the mixing model calibration, although it is evident that soil water contents inferred from permittivity measurements at higher temperatures had greater errors.

Soil water content calibrations were applied to measured temperature, permittivity, and bulk electrical conductivity data in the Ap horizon of the Pullman soil in an instrumented field described by Schwartz et al. (2008). We estimated soil water contents using a measured input spectrum bandwidth ω_S = 2.0 rad GHz (0.318 GHz) and assuming a uniform bulk density of 1.35 Mg m^{-3}. Predicted soil water contents at 0.05 and 0.10 m using the square root of permittivity calibration (Table 7) and using the Topp et al. (1980) equation were characteristically in phase with soil temperatures (Fig. 6b). The magnitudes of the water content oscillations for these empirical models were greatest for the 0.05-m soil depth and ranged from 0.016 to 0.022 m^3 m^{-3} during days without precipitation. The Topp et al. (1980) equation underestimated water

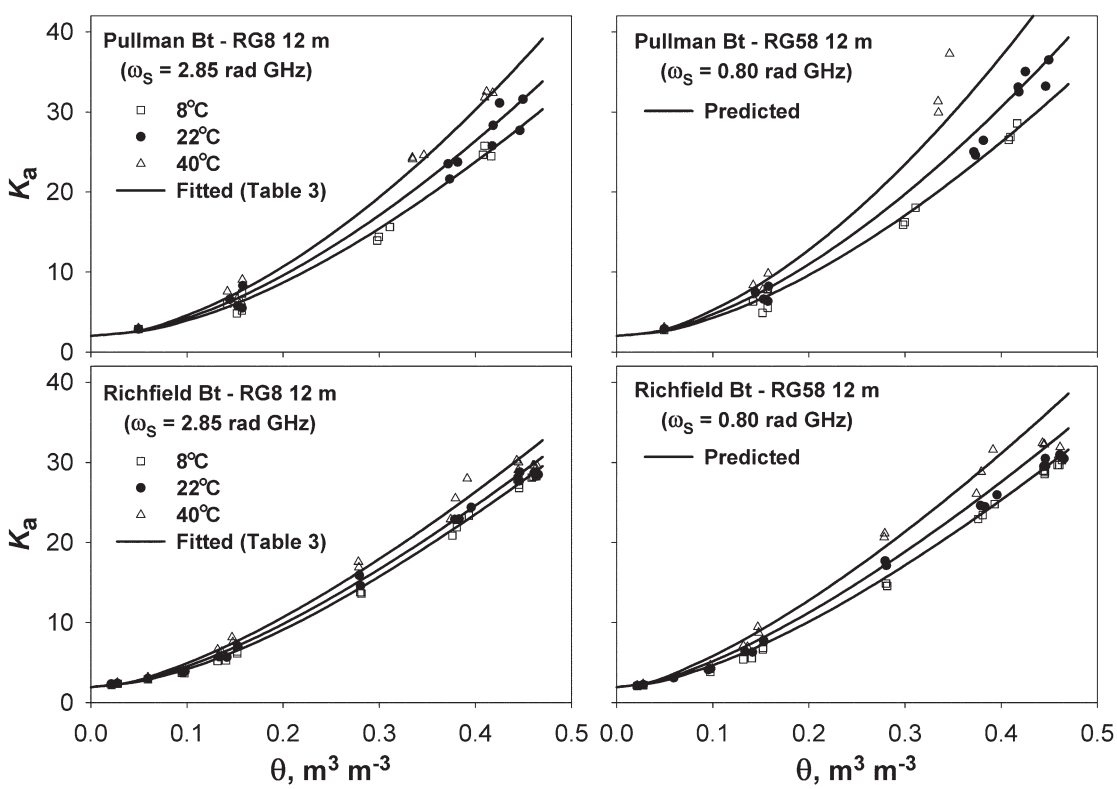

Fig. 4. Measured apparent permittivities (K_a) for the Bt horizons at a range of water contents (θ) and corresponding fitted responses for an input bandwidth (ω_S) of 2.85 rad GHz (0.454 GHz) using the fitted parameters in Table 6b (left). The predicted responses for an input bandwidth of 0.80 rad GHz (127 MHz) (right) are shown using the same fitted parameters (Table 6b). All predicted responses estimate bulk electrical conductivity using the fitted coefficients in Table 1. Some RG 58 cable observations are not shown because of complete attenuation of the second reflection.

Table 7. Linear least square results of the square root of permittivity calibration and RMSE for predicted vs. measured volumetric soil water contents for all cables.

Soil	Square root permittivity empirical calibration†			Mixing model calibration RMSE‡
	b_0	b_1	RMSE	
Pullman Ap	−0.1282	0.1057	0.0212	0.0182
Pullman Bt	−0.0834	0.0912	0.0297	0.0241
Richfield Ap	−0.1352	0.1056	0.0178	0.0090
Richfield Bt	−0.1236	0.1044	0.0196	0.0114

† b_0 and b_1 are the intercept and slope of the linear regression equation, respectively.

‡ Predicted water contents using the mechanistic calibration were obtained by solving for the root of Eq. [9] using the fitted parameters for the power-law dielectric mixing model (Table 6b).

contents at 0.05 m, probably because it was calibrated using soils with lower clay contents and hence smaller fractions of bound water than the Pullman soil.

Using the calibrated mixing model (Table 6b), the predicted water contents at 0.10 m were completely dampened with respect to in-phase temperature oscillations (Fig. 6a). At 0.05 m, diel water content oscillations were reduced to a magnitude <0.004 $m^3\ m^{-3}$ during days without precipitation (Fig. 6a). Dampening of the water content oscillations enabled the detection of small increases (<0.02 $m^3\ m^{-3}$) in soil water content attributed to small precipitation events (<10 mm) that were otherwise masked by diel temperature fluctuations using the empirical calibration. The square root of permittivity calibration yielded mean daily water contents similar to the mixing model, probably because average temperatures during this time period were ~24°C, which approximated the average calibration temperature of 23°C. At higher and lower average temperatures, the square root of permittivity calibration would be expected to overestimate and underestimate, respectively, the soil water contents.

Evett et al. (2005) proposed a square root of permittivity equation with an additional loss term consisting of the measured bulk electrical conductivity and an effective frequency to remove temperature effects from the estimated soil water contents. Using the calibration of Evett et al. (2005, Table 7, Soil A), the predicted water contents at 0.1 m were similar to the dielectric mixing model and completely dampened with respect to in-phase temperature oscillations (Fig. 6d). In contrast, water contents predicted at 0.05 m using the Evett et al. (2005) calibration exhibited oscillations similar to the square root of permittivity calibration (Fig. 6b) and in phase with temperature fluctuations. At the 0.05-m depth, soil water contents are low and the bulk electrical conductivity of the soil becomes small, which results in a negligible loss term and hence temperature dependencies characteristic of the square root of permittivity calibrations. At these low water contents, temperature dependencies arise out of the change in bound water fraction with temperature, which was not considered in the Evett et al. (2005) equation.

Recommended Calibration and Field Implementation Procedure

Based on these results, we propose a generalized calibration of soil water contents with respect to apparent permittivities calculated using Eq. [7] in conjunction with either mixing model (Eq. [2] or [3]) and the approximate effective frequency calculation in Eq. [5]. The procedure (Fig. 7) consists of first calibrating the K_a–θ relationship under controlled conditions in the laboratory, after which the calibration is applied to estimate θ in the field once the physical characteristics of the field setup have been measured. The laboratory calibration should consist of a cable tester, multiplexer, TDR probes with lead coaxial cables of uniform length, and a single primary coaxial cable with a length corresponding to the average length and attenuation rating used in the field. The primary coaxial cable connects the cable tester to the multiplexer and also serves to decrease the signal bandwidth to a value comparable to that achieved in the field. We recommend using good quality coaxial cable such as RG 8 with very low attenuation to minimize errors associated with high-frequency filtering, especially in fine-textured soils. Manufacturer models of the cable tester and multiplexer used in the laboratory calibrations should be equivalent to those deployed in the field. Moreover, all TDR probes are assumed to be geometrically identical.

The laboratory cabling setup is characterized by measuring the air and short-circuit reflection coefficients and probe constant (K_p) (Lin et al., 2008) in addition to the bandwidth ω_S of the TDR signal (Schwartz et al., 2009, Eq. [15]) obtained with an open circuit termination using the lead cable with the TDR probe removed. Use of the Lin et al. (2008) method to adjust the σ_0 calibration for a range of cable resistances (lengths) is recommended rather than the Castiglione and Shouse (2003) procedure, which has since been shown to be incorrect (Lin et al., 2008). Using packed soil columns prepared to achieve a range of θ from air dry to near saturation, travel time measurements and final (long-time) reflection coefficients are measured to calculate $K_a(\theta, T)$

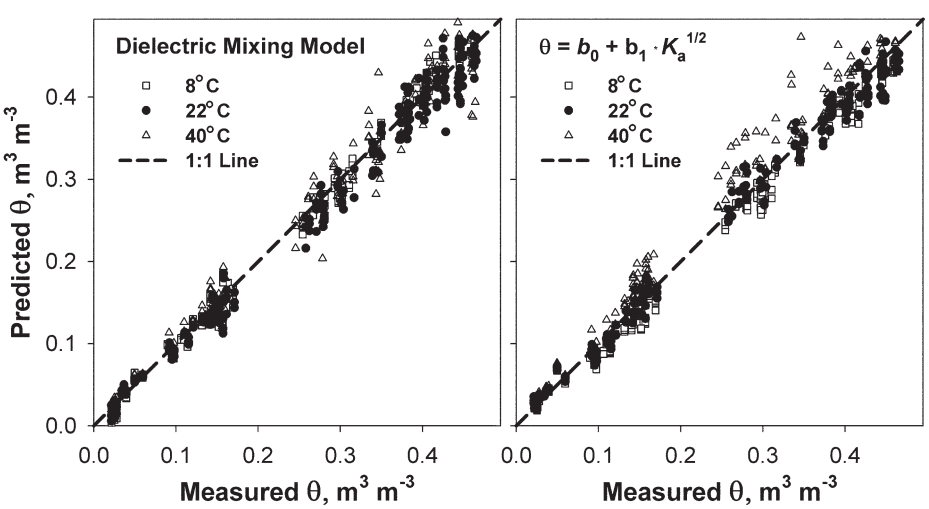

Fig. 5. Measured and predicted water contents (θ) for all cables using the dielectric mixing model calibration (Table 6b) and the square root of permittivity ($K_a^{1/2}$) calibration (Table 7).

and $\sigma_0(\theta,T)$, respectively, at three equilibration temperatures (>4°C). The soil temperatures should encompass the range expected in the field and should span at least 30°C to permit a measurable change in bound water. Lastly, for each representative soil horizon, the specific surface area A_s and polarization loss factor p are fitted based on the objective function Eq. [8] with predicted permittivities based on the measured θ, T, σ_0, ρ_b, and ω_S. If the power-law mixing model is fitted, we recommend using a fixed exponent of $0.55 < a < 0.70$, which encompasses the experimental range in this work together with Dobson et al. (1985) and Or and Wraith (1999).

The estimation of water contents in the field requires first characterizing the cabling setup by measuring the air and short-circuit reflection coefficients together with the ω_S of the TDR signal for each multiplexer with channels occupied by probes. These measurements need to be performed only on a single channel per multiplexer because of the equivalent electrical path lengths for all channels (e.g., Evett, 1998). If coaxial cables between the primary and secondary multiplexers are of similar length and attenuation ratings, then these measurements should be similar in magnitude barring any attenuation caused by moisture, poor contacts, or damaged cable. Once the field setup has been characterized and the soil bulk density has been measured or estimated, field θ can be estimated using the iterative method Eq. [9] with temporal measurements of K_a, σ_0, and T for buried probes in conjunction with the calibration parameters A_s and p for each soil horizon.

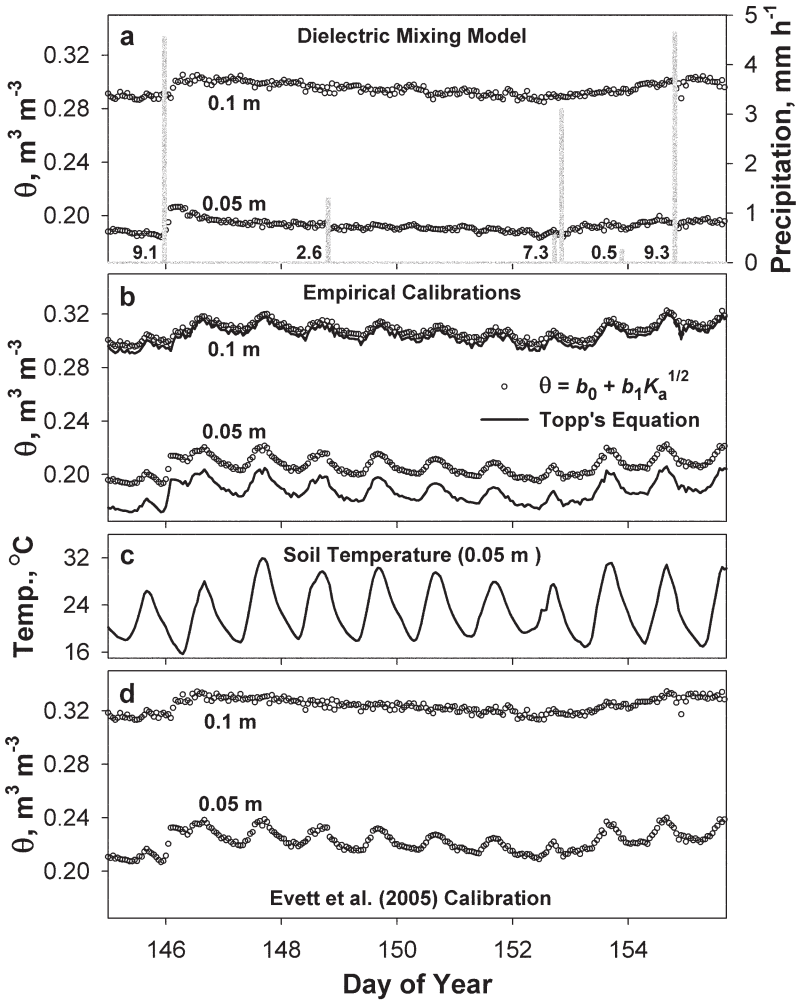

Fig. 6. Field-measured (a) precipitation and (c) soil temperature and estimated water contents (θ) based on (a) the calibrated (Table 6b) dielectric mixing model, (b) the square root of permittivity ($K_a^{1/2}$) calibration and the Topp et al. (1980) equation, and (d) a calibration that considers bulk electrical conductivity effects proposed by Evett et al. (2005, Table 7, Soil A). Measurements are for the Pullman Ap horizon in an instrumented field described by Schwartz et al. (2008).

SUMMARY AND CONCLUSIONS

A four-phase complex dielectric mixing model was calibrated to estimate the apparent permittivity of fine-textured soils using measurements of soil water content, bulk electrical conductivity, temperature, and bulk density. The measured apparent permittivities were best approximated using the power-law dielectric mixing model with a decoupled, semiempirical effective frequency estimate. The power-law exponent was fixed at 0.68 to avoid nonuniqueness problems associated with its positive correlation with the fitted specific surface area. In general, the predicted surface areas increased with increasing clay contents and measured surface areas. The two-parameter mixing model calibration removed temperature bias in the apparent permittivity estimates and reduced the RMSE in the soil water content predictions by an average of 0.006 $m^3\ m^{-3}$ compared with the empirical square root of permittivity calibration. Although apparent permittivity can be estimated across a wide range of loss tangents using the dielectric mixing model developed here, travel time measurement using conventional TDR for these fine-textured soils is imprecise at large (>1.7) loss tangents. We also note that calibrations are dependent on the particular algorithms used for travel time estimation.

Interfacial polarization at the particle–solution interfaces (such as the Maxwell–Wagner effect) are not included in the proposed dielectric mixing model. Consequently, the strong frequency dependence of both the real and imaginary permittivity generated by these processes at frequencies less than about 100 MHz (Ishida et al., 2000; Chen and Or, 2006) is not simulated. Ignoring these processes may explain why the predicted effective frequency based on the direct calculation of attenuation using the dielectric mixing model resulted in poorer estimates of apparent permittivity than the fitted empirical frequency calculation. These uncertainties highlight the need for future studies examining the temperature-dependent dielectric spectroscopy of saturated and unsaturated soils across a wide range of frequencies.

One of the earliest studies investigating the feasibility of high-frequency electromagnetic techniques to measure soil water content (Birchak et al., 1974) suggested that such methods were promising provided that the calculation of the effective dielectric constant could be compensated using measurements of conductivity and temperature. Based on our study, complementary measurements of soil temperature and bulk electrical conductivity are required for high-accuracy (error $\lesssim$0.03 $m^3\ m^{-3}$) soil water content measurements in the field for soils with significant quantities of high-surface-area clays. Under nonisothermal conditions, empirical calibrations will give biased soil water content estimates. As demonstrated by Schwartz et al. (2009), the magnitude and sign

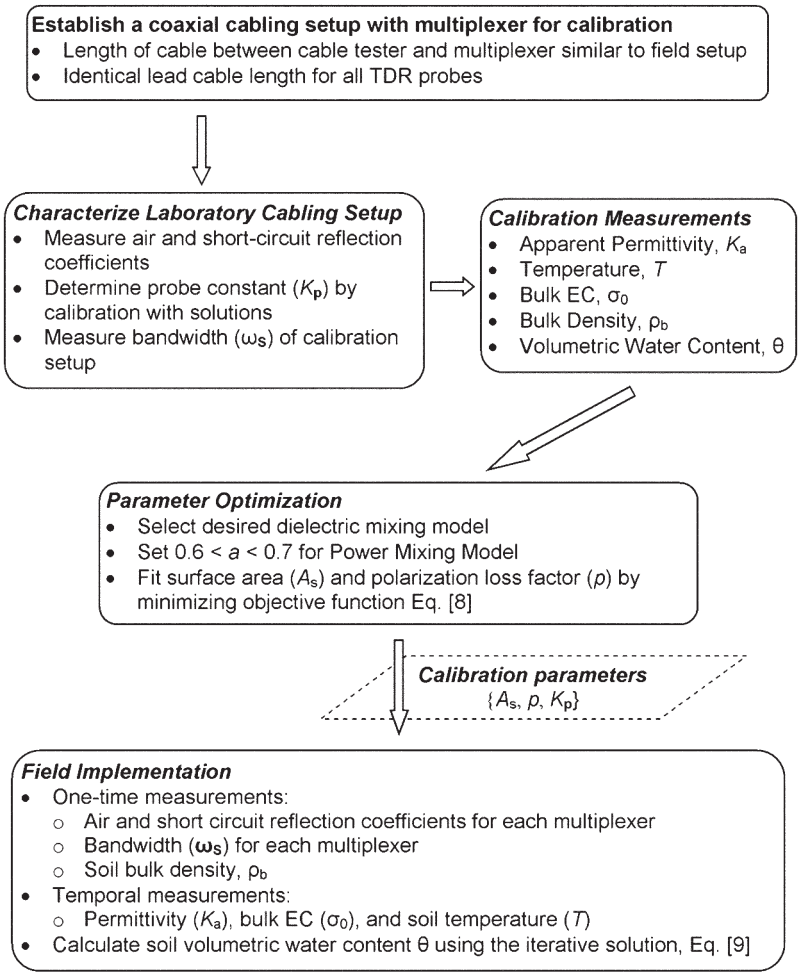

Fig. 7. Flow chart detailing the generalized calibration procedure and field implementation of the complex permittivity model for soil water content sensing.

of the slope of the response of apparent permittivity to temperature depends on the interdependent effects of the relaxation times for bulk and bound water as well as the magnitude of the bulk electrical conductivity. Such a multifaceted temperature response is not easily accommodated using purely empirical expressions.

The dielectric mixing model calibration was evaluated under field conditions during periods of significant temperature fluctuations and small precipitation events. Empirical models predicted water contents with diel oscillations in phase with measured soil temperatures. In contrast, the mixing model removed in-phase fluctuations at 0.1 m and dampened these oscillations to <0.004 $m^3\ m^{-3}$ at the 0.05-m soil depth. Dampening of the temperature-induced oscillations in water content permitted the detection of small (<0.02 $m^3\ m^{-3}$) increases in soil water content attributed to small precipitation events.

ACKNOWLEDGMENTS

We gratefully acknowledge Sally Logsdon and Guy Serbin for the helpful exchanges and reviews of an earlier version of this manuscript. Alan Schlegel kindly provided samples of the Richfield loam for use in the study. In addition, special thanks are extended to Amanda McCarthy for her assistance in the laboratory and with waveform collection.

REFERENCES

Benson, C.H., and X. Wang. 2006. Temperature-compensating calibration procedure for water content reflectometers. Pap. 50. *In* Proc. TDR 2006: Int. Symp. and Worksh. on Time Domain Reflectometry for Innovative Soils Applications, 3rd, West Lafayette, IN. 17–20 Sept. 2006. Available at engineering.purdue.edu/TDR/Papers/50_Paper.pdf (verified 10 Feb. 2009). College of Eng., Purdue Univ., West Lafayette, IN.

Birchak, J.R., C.G. Gardner, J.E. Hipp, and J.M. Victor. 1974. High dielectric constant microwave probe for sensing soil moisture. Proc. IEEE 62:93–98.

Borchardt, G. 1989. Smectites. p. 675–727. *In* J.B. Dixon and S.B. Weed (ed.) Minerals in soil environments. 2nd ed. SSSA Book Ser. 1. SSSA, Madison, WI.

Boyarskii, D.A., V.V. Tikhonov, and N.Yu. Komarova. 2002. Model of dielectric constant of bound water in soil for applications of microwave remote sensing. Prog. Electromagnetic Res. 35:252–269.

Castiglione, P., and P.J. Shouse. 2003. The effect of ohmic cable losses on time-domain reflectometry measurements of electrical conductivity. Soil Sci. Soc. Am. J. 67:414–424.

Chen, Y., and D. Or. 2006. Geometrical factors and interfacial processes affecting complex dielectric permittivity of partially saturated porous media. Water Resour. Res. 42:W06423, doi:10.1029/2005WR004744.

de Loor, G.P. 1968. Dielectric properties of heterogeneous mixtures containing water. J. Microw. Power 3–2:67–73.

Dennis, J.E., D.M. Gay, and R.E. Welsch. 1981. An adaptive nonlinear least-squares algorithm. ACM Trans. Math. Softw. 7:348–368.

Dennis, J.E., and R.B. Schnabel. 1983. Numerical methods for unconstrained optimization and nonlinear equations. Prentice Hall, Englewood Cliffs, NJ.

Dirksen, C., and S. Dasberg. 1993. Improved calibration of time domain reflectometry soil water measurements. Soil Sci. Soc. Am. J. 57:660–667.

Dobson, M.C., F.T. Ulaby, M.T. Hallikainen, and M.A. El-Rayes. 1985. Microwave dielectric behavior of wet soil: II. Dielectric mixing models. IEEE Trans. Geosci. Remote Sens. 23:35–46.

Evett, S.R. 1998. Coaxial multiplexer for time domain reflectometry measurement of soil water content and bulk electrical conductivity. Trans. ASAE 41:361–369.

Evett, S.R. 2000a. The TACQ program for automatic time domain reflectometry measurements: I. Design and operating characteristics. Trans. ASAE 43:1939–1946.

Evett, S.R. 2000b. The TACQ program for automatic time domain reflectometry measurements: II. Waveform interpretation methods. Trans. ASAE 43:1947–1956.

Evett, S.R., J.A. Tolk, and T.A. Howell. 2005. Time domain reflectometry calibration in travel time, bulk electrical conductivity, and effective frequency. Vadose Zone J. 4:1020–1029.

Fanning, D.S., V.Z. Keramidas, and M.A. El-Desoky. 1989. Micas. p. 551–634. *In* J.B. Dixon and S.B. Weed (ed.) Minerals in soil environments. 2nd ed. SSSA Book Ser. 1. SSSA, Madison, WI.

Ferré, P.A., and G.C. Topp. 2002. Time domain reflectometry. p. 434–446. *In* J.H. Dane and G.C. Topp (ed.) Methods of soil analysis. Part 4. Physical methods. SSSA Book Ser. 5. SSSA, Madison, WI.

Friedman, S.P., S.B. Jones, and D.A. Robinson. 2006. Plenary lecture: Review of geometrical and interfacial factors determining effective permittivity–volumetric water content relationships of soils and rocks. *In* Proc. TDR 2006: Int. Symp. and Worksh. on Time Domain Reflectometry for Innovative Soils Applications, 3rd, West Lafayette, IN. 17–20 Sept. 2006. Available at engineering.purdue.edu/TDR/Papers/48_Paper.pdf (verified 10 Feb. 2009). College of Eng., Purdue Univ., West Lafayette, IN.

Gee, G.W., and D. Or. 2002. Particle-size analysis. p. 255–293. *In* J.H. Dane and G.C. Topp (ed.) Methods of soil analysis. Part 4. Physical methods. SSSA Book Ser. 5. SSSA, Madison, WI.

Gong, Y., Q. Cao, and Z. Sun. 2003. The effects of soil bulk density, clay content and temperature on soil water content measurement using time-domain reflectometry. Hydrol. Processes 17:3601–3614.

Greenspan, L. 1977. Humidity fixed points of binary saturated aqueous

solutions. J. Res. Natl. Bur. Stand., Sect. A 81:89–96.
Heimovaara, T.J. 1993. Design of triple-wire time domain reflectometry probes in practice and theory. Soil Sci. Soc. Am. J. 57:1410–1417.
Heimovaara, T.J., W. Bouten, and J.M. Verstraten. 1994. Frequency domain analysis of time domain reflectometry waveforms: 2. A four-component complex dielectric mixing model for soils. Water Resour. Res. 30:201–209.
Herkelrath, W.N., S.P. Hamburg, and F. Murphy. 1991. Automatic real-time monitoring of soil moisture in a remote field area with time domain reflectometry. Water Resour. Res. 27:857–864.
Hook, W.R., T.P.A. Ferré, and N.J. Livingston. 2004. The effects of salinity on the accuracy and uncertainty of water content measurements. Soil Sci. Soc. Am. J. 68:47–56.
Ishida, T., T. Makino, and C. Wang. 2000. Dielectric-relaxation spectroscopy of kaolinite, montmorillonite, allophane, and imogolite under moist conditions. Clays Clay Miner. 48:75–84.
Jacobsen, O.H., and P. Schjønning. 1993. A laboratory calibration of time domain reflectometry for soil water measurement including effects of bulk density and texture. J. Hydrol. 151:147–157.
Kahimba, F.C., and R.S. Ranjan. 2007. Soil temperature correction of field TDR readings obtained under near freezing conditions. Can. Biosyst. Eng. 49:19–26.
Kaiser, K.L. 2005. Electromagnetic compatibility handbook. CRC Press, Boca Raton, FL.
Kelleners, T.J., R.W.O. Soppe, D.A. Robinson, M.G. Schaap, J.E. Ayars, and T.H. Skaggs. 2004. Calibration of capacitance probe sensors using electric circuit theory. Soil Sci. Soc. Am. J. 68:430–439.
Ledieu, J., P. de Ridder, P. de Clerck, and S. Dautrebande. 1986. A method of measuring soil moisture by time-domain reflectometry. J. Hydrol. 88:319–328.
Lin, C.-P., C.C. Chung, J.A. Huisman, and S.-H. Tang. 2008. Clarification and calibration of reflection coefficient for electrical conductivity measurement by time domain reflectometry. Soil Sci. Soc. Am. J. 72:1033–1040.
Logsdon, S.D. 2000. Effect of cable length on time domain reflectometry calibration for high surface area soils. Soil Sci. Soc. Am. J. 64:54–61.
Logsdon, S.D. 2005. Time domain reflectometry range of accuracy for high surface area soils. Vadose Zone J. 4:1011–1019.
Logsdon, S.D. 2006. Experimental limitations of time domain reflectometry hardware for dispersive soils. Soil Sci. Soc. Am. J. 70:537–540.
Malicki, M.A., R. Plagge, and C.H. Roth. 1996. Improving the calibration of dielectric TDR soil moisture determination taking into account the solid soil. Eur. J. Soil Sci. 47:357–366.
Mironov, V.L., M.C. Dobson, V.H. Kaupp, S.A. Komarov, and V.N. Kleshchenko. 2004. Generalized refractive mixing dielectric model for moist soils. IEEE Trans. Geosci. Remote Sens. 42:773–785.
Newman, A.C.D. 1983. The specific surface of soils determined by water sorption. J. Soil Sci. 34:23–32.
Or, D., and J.M. Wraith. 1999. Temperature effects on soil bulk dielectric permittivity measured by time domain reflectometry: A physical model. Water Resour. Res. 35:371–383.
Pennell, K.D. 2002. Specific surface area. p. 295–315. *In* J.H. Dane and G.C. Topp (ed.) Methods of soil analysis. Part 4. Physical methods. SSSA Book Ser. 5. SSSA, Madison, WI.
Pepin, S., N.J. Livingston, and W.R. Hook. 1995. Temperature-dependent measurement errors in time domain reflectometry determinations of soil water. Soil Sci. Soc. Am. J. 59:38–43.
Persson, M., and R. Berndtsson. 1998. Texture and electrical conductivity effects on temperature dependency in time domain reflectometry. Soil Sci. Soc. Am. J. 62:887–893.
Press, W.H., S. A. Teukolsky, W.T. Vetterling, and B.P. Flannery. 1992. Numerical recipes in FORTRAN: The art of scientific computing. 2nd ed. Cambridge Univ. Press, New York.
Quirk, J.P., and R.S. Murray. 1999. Appraisal of the ethylene glycol monoethyl ether method for measuring hydratable surface area of clays and soils. Soil Sci. Soc. Am. J. 63:839–849.
Robinson, D.A. 2004. Measurement of the solid dielectric permittivity of clay minerals and granular samples using time domain reflectometry immersion method. Vadose Zone J. 3:705–713.
Robinson, D.A., S.B. Jones, J.M. Wraith, D. Or, and S.P. Friedman. 2003. A review of advances in dielectric and electrical conductivity measurement in soils using time domain reflectometry. Vadose Zone J. 2:444–475.
Roth, K., R. Schulin, H. Flühler, and W. Attinger. 1990. Calibration of time domain reflectometry for water content measurements using a composite dielectric approach. Water Resour. Res. 26:2267–2273.
Schwartz, R.C., R.L. Baumhardt, and T.A. Howell. 2008. Estimation of soil water balance components using an iterative procedure. Vadose Zone J. 7:115–123.
Schwartz, R.C., S.R. Evett, M.G. Pelletier, and J.M. Bell. 2009. Complex permittivity model for time domain reflectometry soil water content sensing: I. Theory. Soil Sci. Soc. Am. J. 73:876–887 (this issue).
Soil Survey Staff. 2008. National soil survey characterization data. Available at ssldata.nrcs.usda.gov/ (accessed 9 Apr. 2008, verified 10 Feb. 2009). Soil Surv. Lab., Natl. Soil Surv. Ctr., Lincoln, NE.
Sposito, G., and R. Prost. 1982. Structure of water adsorbed on smectites. Chem. Rev. 82:553–573.
Stogryn, A.P. 1995. The microwave permittivity of sea and fresh water. GenCorp Aerojet, Azusa, CA.
Topp, G.C., J.L. Davis, and A.P. Annan. 1980. Electromagnetic determination of soil water content: Measurements in coaxial transmission lines. Water Resour. Res. 16:574–582.
Topp, G.C., and W.D. Reynolds. 1998. Time domain reflectometry: A seminal technique for measuring mass and energy in soil. Soil Tillage Res. 47:125–132.
Wraith, J.M., and D. Or. 1999. Temperature effects on soil bulk dielectric permittivity measured by time domain reflectometry: Experimental evidence and hypothesis development. Water Resour. Res. 35:361–369.